Journal of Materials Chemistry A

PAPER

View Article Online
View Journal | View Issue

Cite this: J. Mater. Chem. A, 2014, 2, 12526

Solid-state functionalization of graphene with amino acids toward water-dispersity: implications on a composite with polyaniline and its characteristics as a supercapacitor electrode material†

Gansukh Erdenedelger,‡[a] Taemin Lee,‡[b] Trung Dung Dao,‡[a] Joon Soo Kim,[c] Byeong-Su Kim*[b] and Han Mo Jeong*[a]

Received 19th March 2014
Accepted 3rd June 2014

DOI: 10.1039/c4ta01345j

www.rsc.org/MaterialsA

A new and facile modification method to endow graphene with water-dispersity is reported. The remanent epoxide group on graphene prepared by the thermal reduction of graphite oxide is effectively utilized for the modification reaction with the amine group of potassium 6-aminocaproate using a simple process of heating the well-mixed solid state mixture. The graphene modified to have negatively charged carboxylate moieties disperses easily and stably in water. A graphene/polyaniline (PANI) composite is prepared efficiently in an aqueous system by the simple physical mixing of aqueous dispersions of negatively charged graphene and positively charged micron-size PANI particles, followed by drying. The composites exhibit higher energy storage capacities as supercapacitor electrodes compared to those of either graphene or PANI themselves. The synergistic effect is most evident at a graphene/PANI weight ratio of 20/80. The composite exhibits more than twice the specific capacitance of either PANI or graphene. This suggests that the scaffold structure of hydrophilic graphene enclosing PANI particles reduces not only the contact resistance at the electrode/electrolyte interface but also the diffusion length for effective charge transfer.

Introduction

Graphene, a two-dimensional aromatic carbon monolayer, has attracted significant interest in various fields of science and engineering because of its unique and extraordinary electronic, optical, thermal and mechanical properties together with a superior surface area.[1] Along with an understanding of the fundamental physics of graphene, the development of effective means for the mass production of high quality graphene and efficient post-functionalization would make graphene versatile for a range of applications.

Bulk quantities of flake-type graphene can be produced effectively by rapid heating of highly oxidized graphite oxide (GO) powders because GO sheets are reduced and exfoliated simultaneously upon rapid heating due to thermal decomposition of the oxygen-containing groups of GO, and the pressure of gas products (mainly CO_2) that builds up instantaneously at the gallery between the sheets.[2] This method is economical and eco-friendly because high-quality graphene can be mass-produced without the use of a solvent in the reduction process. These exfoliated graphene sheets are normally a few-layer graphene with a specific surface area, ranging from 400 to 1500 $m^2 g^{-1}$, according to the Brunauer, Emmett, and Teller (BET) measurements.[3–5] These exfoliated sheets are called functionalized graphene sheets because they contain some oxygen-containing functional groups, such as epoxide and hydroxyl groups, even after thermal reduction.[5,6] Therefore, these functionalized graphene sheets can be dispersed finely in polar solvents and polymer matrices but they are barely dispersed in water or water-soluble polymers.[3,5,7–9]

Additional modification or functionalization to endow water-dispersity to thermally reduced graphene (TRG) can pave the way toward a range of promising applications because water-dispersity is a prerequisite for many applications. In addition, eco-friendly water can be a substitute for unfavorable solvents in various processes to prepare graphene-based materials. In previously reported studies, GO was reduced after the covalent functionalization of GO with a hydrophilic functional group

[a]Department of Chemistry, Energy Harvest-Storage Research Center, University of Ulsan, Ulsan 680-749, Korea. E-mail: hmjeong@mail.ulsan.ac.kr; Tel: +82-52-259-2343

[b]Department of Chemistry and Department of Energy Engineering, Ulsan National Institute of Science and Technology (UNIST), Ulsan 689-798, Korea. E-mail: bskim19@unist.ac.kr; Tel: +82-52-217-2923

[c]Korea Institute of Energy Research (KIER), Daejeon 305-343, Korea

† Electronic supplementary information (ESI) available. See DOI: 10.1039/c4ta01345j

‡ These authors contributed equally to this paper.

such as a sulfonate group,[10] or a hydrophilic molecule such as poly-L-lysine,[11] or a charged moiety such as ionic liquid[12] to impart water-dispersity. In other cases, GO was reduced in the presence of a dispersing agent, such as poly(sodium-4-styrene sulfonate),[13] pyrenebutyric acid,[14] or porphyrin[15] for non-covalent functionalization. However, such methods usually disrupt the π-bond system of graphene or contaminate graphene's surface with a large amount of macromolecules or surfactants, causing the deterioration or loss of unique properties of graphene in the functionalized one or the introduction of big impurities to the final products.[16] In addition, these methods can barely be applied to graphene prepared by a thermal reduction process because it does not use any solvent and it undergoes a high temperature reduction process. Therefore, challenging endeavors are continuing to develop a convenient means of post-processing to afford water-dispersible graphene.

This paper reports the facile synthesis of water-dispersible graphene through a solid-state reaction between the remanent epoxide group on TRG and the amine group of 6-aminocaproic acid to introduce negatively charged carboxylate groups to the graphene sheet (Scheme 1a). The reaction process is simple because the reaction is carried out effectively in the solid state by simple heating of a reactant mixture. No solvent is necessary at the reaction stage, but solvents for intimate mixing of TRG and 6-aminocaproic acid are necessary only at the preparatory stage. Furthermore, the damage to the intrinsic properties of TRG by covalent modification is minimized because the inherent defect, the remanent epoxide group on graphene, is used as an anchoring site for modification without altering the intact basal plane of graphene.[17,18]

In addition, the stable aqueous dispersity allows the integration of graphene with aqueous polymers to prepare graphene/polymer composites conveniently by the simple physical mixing of aqueous dispersions.[9,18] In this process, the charges on the graphene (or GO) sheets and the counter charges on the polymer particles can promote intimate mixing because electrostatic attractions between the graphene sheets and polymer particles cause the sheets to cover the polymer particle, which also prevents the aggregation of graphene sheets during drying.[19,20]

Polyaniline (PANI) has attracted considerable attention as a supercapacitor electrode material because it has high pseudocapacitance by a redox reaction and the electrode can be fabricated in an aqueous system.[21] Graphene has not only excellent electrical conductivity and mechanical strength, but also a high surface area for the electrical double-layer capacitance that comes from charge accumulation at the electrode/electrolyte interface. Therefore, an appropriately designed graphene/PANI composite can have a synergistic effect on both energy storage mechanisms. Many studies have examined the availability and synergistic effect of graphene/PANI composites as active electrode materials for supercapacitors.[22–28]

In this study, the availability of negatively charged graphene for facile composite preparation in aqueous systems was assessed using a graphene/PANI composite. The negatively charged graphene was mixed simply in water with positively charged micron-sized PANI particles to prepare the composite, where the PANI particles are enclosed in a graphene scaffold, as shown in Scheme 1b, to examine the synergistic effects on the supercapacitor performance.

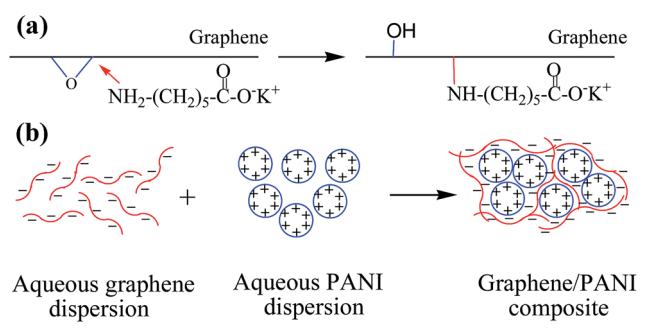

Scheme 1 Schematic diagram of the process to prepare (a) water-dispersible graphene and (b) water-based graphene/PANI composite.

Experimental

Materials

Expandable graphite (ES350 F5, mean particle size of 280 μm) was purchased from Qingdao Kropfmuehl Graphite Co., Ltd. (China) and used for the preparation of graphene. PANI emeraldine salt powder (average molecular weight: >15 000, particle size: 3–100 μm, surface area: 5–20 $m^2\ g^{-1}$, and density: 1.38 g mL^{-1}), Nafion (perfluorinated ion-exchange resin, 5 wt% solution in lower aliphatic alcohols and water), 6-aminocaproic acid, acetone, and KOH were obtained from Aldrich and used as received.

GO was prepared using the Brodie method, as described elsewhere.[29] Briefly, a reaction flask with 200 mL fuming nitric acid was cooled in an ice bath to 0 °C, and 10 g of graphite powder was added under stirring. Over a 1 h period, 85 g of potassium chlorate was then added slowly under stirring at 25 °C. After 24 h, the mixture was poured into 3 L of distilled water. GO was then filtered and washed with distilled water until the pH of the filtrate was neutral. The mixture was then dried in a vacuum oven at 100 °C. The as-prepared GO composition based on elemental analysis was determined to be $C_{10}O_{3.45}H_{1.58}$.

To obtain TRG, the dried GO was charged in a quartz tube and flushed with nitrogen for 5 min. The quartz tube was then inserted rapidly into a furnace preheated to 1100 °C and kept for 1 min for the simultaneous thermal exfoliation and reduction of GO.[2,6] Elemental analysis showed that the composition of TRG was $C_{10}O_{0.78}H_{0.38}$. The specific surface area was 428 $m^2\ g^{-1}$ according to the BET measurement from nitrogen adsorption in the dry state.

Modification of graphene with 6-aminocaproic acid

TRG and potassium 6-aminocaproate were reacted in the solid state to prepare graphene with negatively charged carboxylate moieties, as shown in Scheme 1a. In particular, 13.1 g (0.1 mol) of 6-aminocaproic acid and 5.6 g (0.1 mol) of KOH were

dissolved in 20 g water. The aqueous solution was mixed with TRG (0.5 g) dispersion in acetone (150 mL) for 30 min with an agitator and then sonicated for 45 min. Water and acetone were evaporated, and the remaining well-mixed solid mixture was heated in an oven for 2 days at 90 °C to induce a reaction between the epoxide group on TRG and the amine group of potassium 6-aminocaproate. The resulting reacted mixture was dispersed in a 20-fold volume of hot water and filtered after sonication for 15 min. The filtered solid was washed with hot water and acetone, and dried in a vacuum oven at 50 °C for 1 day to obtain negatively charged, 6-aminocaproic acid-functionalized thermally reduced graphene (C-TRG). In a separate experiment, a control sample (C-TRGM) was prepared using a procedure designed so that potassium 6-aminocaproate can only be absorbed physically on TRG with a marginal reaction. That is, the mixture was filtered before evaporating water and acetone, and the filtered solid was then dried in an oven at 50 °C for 1 day without additional heating at higher temperatures. For comparison, the TRGs modified with other amino acids, such as glycerine (G-TRG) and 11-aminoundecanoic acid (U-TRG), were also prepared using an identical procedure, as described for C-TRG.

Preparation of the graphene/PANI composite

C-TRG was dispersed in 150-fold of water and sonicated for 1 h. PANI was also dispersed in 150-fold of water and sonicated for 10 h. The two dispersions were mixed for 30 min and dried in a vacuum at 60 °C for one day to obtain a graphene/PANI composite (Scheme 1b). In the preparation of composites for electrochemical characterization, a Nafion solution was mixed together as a polymer binder to fabricate the supercapacitor electrode. The solid weight ratio of composite/Nafion was adjusted to 85/15. The sample designation codes of the composites in Fig. 7–9 provide information on the weight ratio of C-TRG/PANI. For example, the weight ratio of C-TRG/PANI in G15/P85 was 15/85.

Preparation of supercapacitor electrodes and electrochemical measurements

The electrochemical measurements were carried out using a standard three-electrode test cell. The C-TRG/PANI composite dispersion mixed with a Nafion solution was drop-cast on a glass carbon electrode (total solid: 60 μg) and dried in a vacuum at room temperature. The electrochemical performance of the electrode was examined using a VMP3 electrochemical potentiostat (BioLogic Inc.). A platinum wire electrode and saturated calomel electrode (SCE) were used as the counter and reference electrodes, respectively. Cyclic voltammetry (CV) was performed and the galvanostatic charge–discharge process was carried out with a potential window from −0.2 to 0.8 V *vs.* SCE in a 0.1 M H_2SO_4 aqueous electrolyte with wide scan rates from 10 to 200 mV s^{-1} and a discharge current density from 0.5 to 3 A g^{-1}.[30] Electrical impedance spectroscopy (EIS) was performed over the frequency range 0.1 Hz−200 kHz.

Characterization

The morphology of the samples was observed using a field-emission scanning electron microscope (FE-SEM, JEOL JSM-6500F) and a transmission electron microscope (TEM, Hitachi H-8100). An atomic force microscopy (AFM) image of graphene was taken using a Veeco Dimension 3100 SPM with a silicon cantilever operated in the tapping mode.

The Fourier transform infrared (FTIR, FTS 2000 FTIR, Varian) spectra were recorded using a KBr tablet that was made by compression molding of KBr powder mixed with a small amount of sample. Elemental analysis of carbon, hydrogen, oxygen, and nitrogen was carried out using a Thermo Scientific Flash 2000 CHNS/O analyzer. X-ray photoelectron spectroscopy (XPS, Thermo Fisher K-Alpha) was performed on a spectrometer using Al Kα X-ray radiation. The Raman spectra of graphene paper were recorded using a Raman spectrometer (WITec, Alpha 300R) equipped with a microscope (50× objective) and a Nd-YAG laser with an excitation wavelength of 532 nm. Thermogravimetric analysis (TGA, Q50 TA Instrument) was performed at a heating rate of 10 °C min^{-1} with a 2 mg sample in a platinum crucible under a N_2 atmosphere. The electrical conductivity of the pressed graphene powder (density ≈ 0.6 g cm^{-3}) was measured using a two-probe method on a Keithley 237 source-measure unit at room temperature.

Results and discussion

Analysis of 6-aminocaproic acid-functionalized, thermally reduced graphene (C-TRG)

The morphology and topography of TRG and C-TRG were characterized using SEM, TEM and AFM as shown in the ESI (Fig. S1†). The SEM and TEM images of TRG and C-TRG show that the graphenes are ultra-thin graphene sheets with a lateral size of several micrometers and with a wrinkled morphology which is typical for thermally reduced graphene.[6] The AFM image was observed on a silicon substrate. Because most of the fraction of the graphene sheet was not in contact with the substrate due to the wrinkled morphology of graphene, the thickness of the sheet has been measured at the edge thereof to be less than 1 nm, indicating single-layer graphene.[2]

The superior dispersity and stability of the prepared C-TRG in water were verified after the functionalization of thermally reduced graphene with 6-aminocaproic acid. TRG was difficult to disperse and it settled immediately when attempts were made to disperse it in water by sonication. On the other hand, C-TRG dispersed readily in water and the homogeneous colloidal dispersion of C-TRG (0.1 mg mL^{-1}) was stable for more than two months without significant aggregation (Fig. 1). This shows that the carboxylate groups on graphene effectively improved the hydration of the graphene surface. In addition, the wrinkled nature of graphene[2,29] as well as the electrostatic repulsion between the graphene sheets caused by the ionic sites of 6-aminocaproate functionalized on the surface of C-TRG efficiently prevented graphene from restacking and aggregation.[31,32] In comparison, when the modification reaction was carried out in the mixed solvents of water and acetone (or other

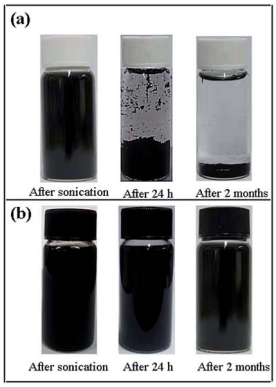

Fig. 1 Photographs of aqueous dispersions of (a) TRG and (b) C-TRG.

solvents, such as dimethylformamide), instead of in the solid state, the colloidal stability of the modified TRG was poorer than that of C-TRG. This can be attributed to the poor solubility of potassium 6-aminocaproate and/or the poor dispersity of TRG, which limit complete mixing of the two components, resulting in inefficient modification reactions. A liquid medium that is compatible for both TRG and potassium 6-aminocaproate was difficult to find. This highlights the utility of a solid-state reaction during the modification of TRG.

The aqueous colloidal stability of the TRGs modified with other amino acids, such as glycerin (G-TRG) or 11-aminoundecanoic acid (U-TRG), was also compared. The colloidal stability of these modified TRGs was poorer than that of C-TRG. That is, a considerable amount of U-TRG and an even larger amount of G-TRG had settled before 1 month. Since the amounts of amino acids attached to TRG, which was estimated by TGA, were not significantly different (see the discussion on TGA) from that of C-TRG, it was assumed that the molecular size or the molecular shape of the attached amino acid moiety can affect the colloidal stability of modified TRG. Nevertheless, further study will be needed for systematic explanation.

The FTIR spectrum of potassium 6-aminocaproate exhibits characteristic IR absorption bands for carboxylate groups at 1560 cm^{-1} and 1435 cm^{-1} due to asymmetric and symmetric CO_2 stretching, respectively (Fig. 2a). The spectrum also exhibits a small absorption band for NH_2 stretching at 3360 cm^{-1}. The doublet band at 2925 cm^{-1} and 2853 cm^{-1} was assigned to the asymmetric and symmetric stretching bands, respectively, of the CH_2 group.[33] The FTIR spectrum of TRG has broad IR absorption bands at approximately 1541 cm^{-1} and 1187 cm^{-1}, which were attributed to the C=C bond and C–O bond, respectively (Fig. 2b). The graphene-modified with potassium 6-aminocaproate, C-TRG, has additional peaks from the potassium 6-aminocaproate moiety (Fig. 2c). For example, CH_2 doublet bands at 2925 cm^{-1} and 2853 cm^{-1} and an NH absorption band at 3360 cm^{-1} were observed. In addition, the peak of TRG at approximately 1541 cm^{-1} was shifted to a slightly higher wavenumber to 1567 cm^{-1} due to the contribution of a carboxylate group peak of potassium 6-aminocaproate attached to graphene. On the other hand, the control sample, C-TRGM (Fig. 2d), exhibited a weak CH_2 doublet band only in addition to those bands for TRG. The FTIR spectra showed that potassium 6-aminocaproate has attached effectively by a reaction on C-TRG, as shown in Scheme 1a, whereas a much smaller amount of potassium 6-aminocaproate was attached to C-TRGM.

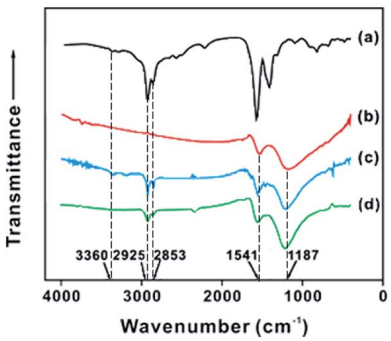

Fig. 2 FTIR spectra of (a) potassium 6-aminocaproate, (b) TRG, (c) C-TRG, and (d) C-TRGM.

Elemental analysis showed that the elemental ratio of C/O/H/N was $C_{10}O_{0.78}H_{0.38}$ for TRG and $C_{10}O_{1.47}H_{4.45}N_{0.31}$ for C-TRG. This shows that TRG consists of carbon, oxygen, and hydrogen, suggesting that some oxygen-containing functional groups, such as epoxide or hydroxyl groups, remained even after thermal reduction.[2,6] On the other hand, an analysis of C-TRG revealed the presence of nitrogen and an increase in the relative amounts of oxygen and hydrogen compared to those of TRG, which confirmed the attachment of potassium 6-aminocaproate to graphene (Scheme 1a).

Fig. 3 shows the C_{1s} core level photoemission spectra of graphene. The asymmetric photoelectron peak could be deconvoluted into five components, as shown in Fig. 3; the peaks attributed to C–C, C–N, C–O, C=O, and O=C–O carbon.[34] Table 1 lists the results of peak deconvolution, including the peak position and percentage of each peak area. An additional contribution of C–N carbon was observed in C-TRG, which is not in TRG. In addition, the number of carbon atoms bonded to the heteroatoms increased, whereas that of the C–C bond decreased in C-TRG compared to that of TRG by the reaction with potassium 6-aminocaproate. These results show that potassium 6-aminocaproate is indeed attached to C-TRG.

Fig. 4 shows the O_{1s} core level photoemission spectra of graphene. Because the oxygen that is doubly bonded to carbon

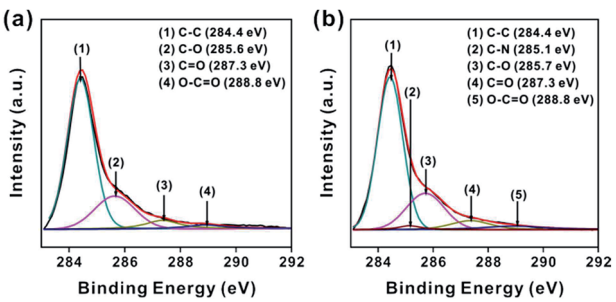

Fig. 3 XPS spectra at the C_{1s} region of (a) TRG and (b) C-TRG.

Table 1 XPS data analysis of the C_{1s} region for graphene

	C–C carbon		C–N carbon		C–O carbon		C=O carbon		O–C=O carbon	
Sample	Peak (eV)	Area (%)	Peak (eV)	Area (%)	Peak (eV)	Area (%)	Peak (eV)	Area (%)	Peak (eV)	Area (%)
TRG	284.4	68.1	—	—	285.6	21.9	287.3	6.6	288.8	3.4
C-TRG	284.4	63.5	285.1	2.2	285.7	22.5	287.3	6.8	288.8	5.0

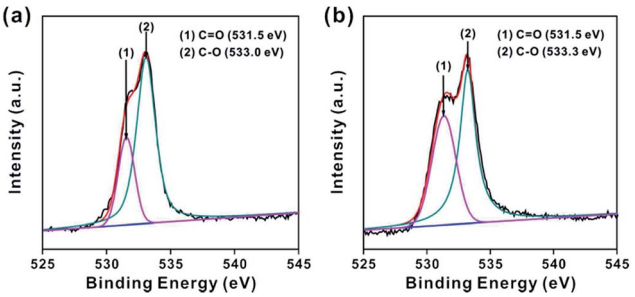

Fig. 4 XPS spectra at the O_{1s} region of (a) TRG and (b) C-TRG.

(C=O oxygen) has a peak at approximately 531 eV and the oxygen that is singly bonded to carbon (C–O oxygen) has a peak at approximately 533 eV,[35] the asymmetric photoelectron peak was deconvoluted into two peaks, as shown in Fig. 4. Table 2 summarizes the results of this peak deconvolution. This shows that C-TRG has a higher amount of C=O oxygen and a lower amount of C–O oxygen compared to those of TRG. This also demonstrates that potassium 6-aminocaproate is attached to C-TRG.

The Raman spectrum of pristine graphene has a characteristic G band at approximately 1580 cm^{-1}.[36] If defects are present on graphene, the D band at approximately 1350 cm^{-1} can be observed. The intensity of the D band is a measure of the amount of disorder in graphene because activation of the D band can be attributed to the breaking of the translational symmetry of the C=C sp^2 bond.[37] Therefore, an increase in the number of defects would result in an increase in the D band intensity and a concomitant drop in the intensity of the intrinsic G band of graphene.[36] Fig. 5 shows that the intensity ratio of the G band relative to the D band, *i.e.* I_G/I_D, is changed marginally by the modification reaction. This result demonstrates that the modification reaction does not damage the conjugated sp^2 C=C network of graphene because the intrinsic defect of graphene, the remnant epoxide group, was used for the reaction.[37]

Fig. 6a shows that the weight loss of TRG observed by TGA at 700 °C was only 1.8%, whereas the weight loss of potassium 6-aminocaproate was as much as 60.6% (Fig. 6d). This shows that TRG is thermally stable, whereas potassium 6-aminocaproate is thermally labile at this temperature. Therefore, the amount of potassium 6-aminocaproate attached to graphene (x_t%) can estimated using eqn (1) if one assumes that the weight loss increases in C-TRGM (Fig. 6b) and C-TRG (Fig. 6c) compared to that of TRG (Fig. 6a) are due mainly to the degradation of thermally labile potassium 6-aminocaproate attached to graphene.

$$\frac{x_t}{100}w_1 + \frac{100 - x_t}{100}w_2 = w_3 \quad (1)$$

Eqn (1) shows that the weight loss of C-TRGM or C-TRG (w_3%) at 700 °C (Fig. 6b or 6c) is a sum of the weight loss of potassium 6-aminocaproate on graphene (the first term of

Table 2 XPS data analysis of the O_{1s} region for graphene

	C=O oxygen		C–O oxygen	
Sample	Peak (eV)	Area (%)	Peak (eV)	Area (%)
TRG	531.5	26.5	533.0	73.5
C-TRG	531.3	41.6	533.2	58.4

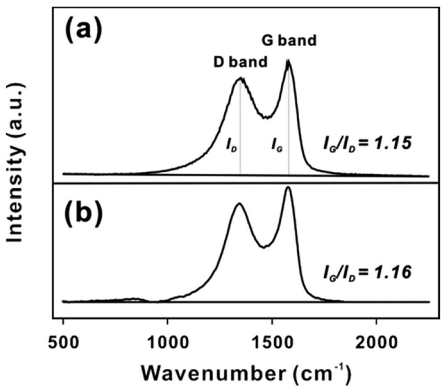

Fig. 5 Raman spectra of (a) TRG and (b) C-TRG.

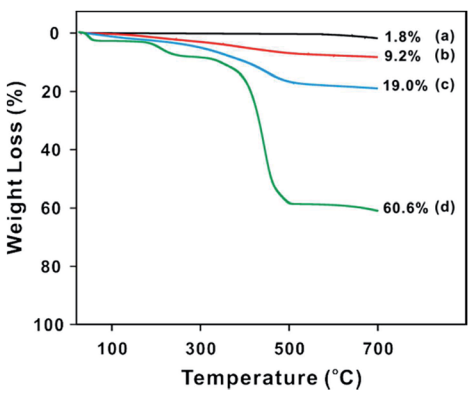

Fig. 6 TGA thermograms of (a) TRG, (b) C-TRGM, (c) C-TRG, and (d) potassium 6-aminocaproate.

eqn (1)) and graphene itself (the second term of eqn (1)) at 700 °C. w_1 (%) and w_2 (%) in eqn (1) are the weight losses at 700 °C of potassium 6-aminocaproate (60.6%, Fig. 6d) and TRG (1.8%, Fig. 6a), respectively. The calculated x_t values for C-TRGM and C-TRG were 12.6% and 29.3%, respectively. These results also show that potassium 6-aminocaproate is indeed functionalized on the surface of C-TRG by solid-state modification reaction. In addition, the x_t values for G-TRG and U-TRG were 31.2% and 29.5%, respectively. The calculations based on these x_t values showed that 0.40, 0.25 and 0.18 moles of amino acids for G-TRG, C-TRG, and U-TRG were attached to 100 g of modified graphene, respectively. These results show that the number of attached amino acids does not depend significantly on the kind of amino acid.

The electrical conductivity of C-TRG compacts (14.4 S cm^{-1}) was lower than that of TRG (26.8 S cm^{-1}). Because the conjugated sp^2 C=C bond system of graphene was not damaged by the modification reaction (Fig. 5), this decrease in electrical conductivity might be due to the limited intimate contact between the graphene sheets in the compact state by the attached 6-aminocaproate moiety, which is electrically insulating.

Analysis of graphene/PANI composite

Fig. 7 shows images of the PANI and the C-TRG/PANI composites. PANI is a micron-size aggregate of sub-micron PANI particles (Fig. 7a). For G15/P85 (Fig. 7b), the C-TRG sheets are well dispersed in the matrix made from the PANI particles, some of them covering the PANI particles. At a higher C-TRG content (Fig. 7c), C-TRG forms a continuous network and PANI particles are enclosed in the scaffold of C-TRG. At an even higher C-TRG content (Fig. 7d), almost all PANI particles were encapsulated by C-TRG sheets without any exposed particles.

To examine the effects of the C-TRG/PANI composite morphology on energy storage, CV was conducted at various weight ratios of C-TRG and PANI (Fig. 8). In addition, pure TRG, C-TRG, and PANI electrodes were also examined to confirm the synergistic effect of the graphene/PANI hybrid architecture. All experiments were conducted over the potential range −0.2–0.8 V (*vs.* SCE), in 0.1 M aqueous H_2SO_4 electrolytes. The specific capacitance (C_{sp}, F g^{-1}) of the electrode can be expressed using eqn (2):

$$C_{sp} = \frac{1}{mv(V_f - V_i)} \int_{V_i}^{V_f} I(V)\mathrm{d}V \quad (2)$$

where I is the response current (A), V_f and V_i are the integration potential (V) limits of the voltammetry curve, v is the potential scan rate (V s^{-1}), and m is the total mass of active materials (C-TRG and PANI) on the electrode (g). Based on the above equation, the C_{sp} of the active materials was estimated from the integrated area in the *I–V* characteristic curves. In Fig. 8a and b, the TRG and C-TRG with no PANI exhibited a symmetric and rectangular shape without an obvious redox peak, which corresponds to the ideal electric double-layer capacitive behavior. In particular, the water-dispersible C-TRG electrode showed much higher electrochemical performance than TRG

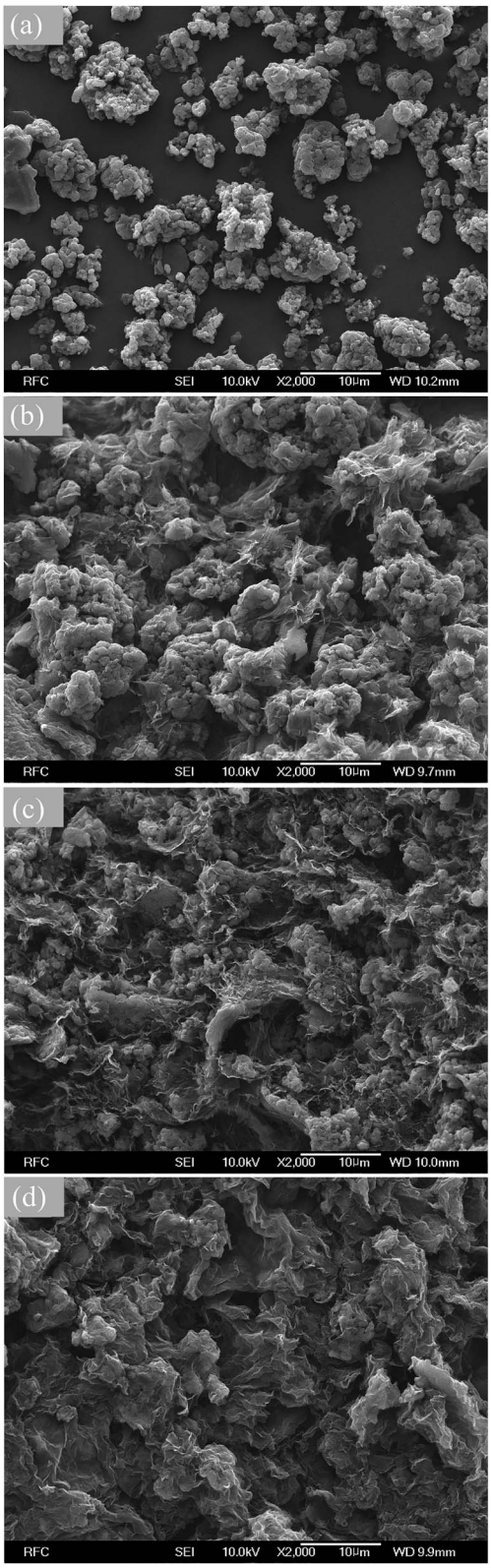

Fig. 7 SEM images of (a) PANI, (b) G15/P85, (c) G20/P80, and (d) G50/P50.

(85.95 F g^{-1} *vs.* 48.57 F g^{-1} at 10 mV s^{-1}), owing to the effective ion accessibility in an aqueous electrolyte. In contrast, PANI itself shows typical pseudocapacitive behavior with two

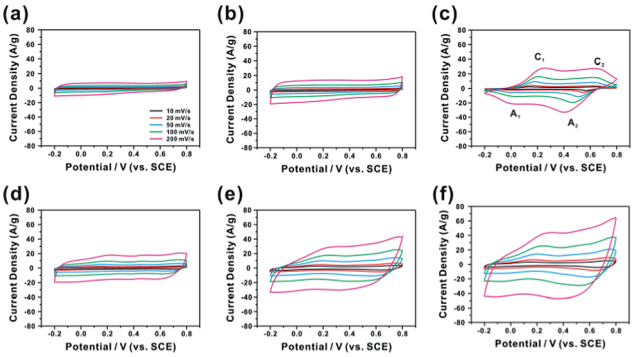

Fig. 8 Cyclic voltammetry curves of (a) TRG, (b) C-TRG, (c) PANI, (d) G80/P20, (e) G40/P60, and (f) G20/P80 electrodes with a wide range of scan rates from 10 to 200 mV s^{-1}. All electrochemical properties were collected in a three-electrode system with potentials from −0.2 to 0.8 V *versus* a SCE reference in a 0.1 M H_2SO_4 electrolyte.

characteristic redox peaks (C_1/A_1 and C_2/A_2) related to the redox transition of PANI (Fig. 8c). The peaks for C_1/A_1 were assigned to the redox transition of PANI between a semiconducting state (leucoemeraldine) and a conducting state (polaronic emeraldine), and the additional redox peaks for C_2/A_2 were associated with the Faradaic transformation of emeraldine to pernigraniline.[38,39] All the composite electrodes displayed intermediate capacitive behavior with two characteristic redox peaks, which appeared remarkably as an increasing portion of PANI in the composite electrodes (Fig. 8d–f). The C_{sp}s of the composites were mostly higher than those of C-TRG or PANI. This synergistic effect on energy storage was most evident at the C-TRG/PANI composition of 20/80 (noted as G20/P80) (Fig. 9c).

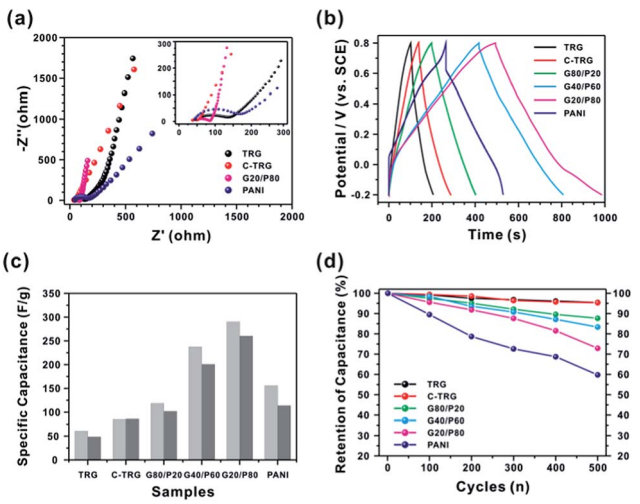

Fig. 9 (a) Nyquist plot of the graphene/PANI composite electrode over the frequency range 0.1 Hz to 200 kHz. The inset shows the enlarged high-frequency region of the plot. (b) Galvanostatic charge–discharge curves of the all-prepared electrodes in this study at a current density of 0.5 A g^{-1}. (c) Specific capacitance from the charge–discharge curves at a 0.5 A g^{-1} discharge current density (left bar) and CV curves at a 10 mV s^{-1} scan rate (right bar). (d) Comparison of the cycling stability at a high discharge current density of 3 A g^{-1}.

This suggests that C-TRG enclosing the PANI particles effectively reduces the diffusion length and induces rapid charge transfer at the interface between the electrodes and the electrolyte. Therefore, the energy storage capability by the pseudocapacitive PANI particles is enhanced significantly.

Electrochemical impedance spectroscopy (EIS) was performed to examine the interfacial resistance of the composite electrodes (Fig. 9a). From the Nyquist plot, the vertical straight line observed in the low frequency region indicates ion diffusion at the electrode/electrolyte interfaces, which corresponds to the representative capacitive behavior.[40,41] In addition, the semi-circle line in the high frequency region corresponds to the electronic resistance between the electrode and the electrolyte. This shows that the C-TRG electrode has lower resistance (~10.5 Ω) than the TRG electrode (~51.5 Ω) and the G20/P80 composite electrode possesses a much lower resistance (~21.5 Ω) than the PANI (~98.5 Ω) electrodes. This suggests that the resistance of TRG was reduced by modification with 6-aminocaproate to endow water-dispersity because of the effective contact with the aqueous electrolyte. Moreover, this highly conducting C-TRG nanosheet, which produces a network structure in the composite, effectively reduces the contact resistance of the C-TRG/PANI composite.

Galvanostatic charge–discharge tests were carried out to further explore the ability and long-term stability of the C-TRG/PANI composite for a supercapacitor. To evaluate the characteristics of intrinsic electrode materials, we measured in a three-electrode system. According to the report of the Ruoff group, a three-electrode cell is valuable for determining electrochemical-specific material characteristics, whereas a two-electrode test cell mimics the physical configuration, internal voltages and charge transfer that occurs in a packaged cell and thus provides the best indication of an electrode performance.[42] Fig 9b shows the galvanostatic charge–discharge profiles for a supercapacitor at a constant current density of 0.5 A g^{-1}. All the prepared electrodes showed ideal capacitive behavior with symmetric responses and a small internal resistance drop, except for pure PANI with a large IR drop due to the instability and poor wettability on the surface of the electrode. The discharge time increased significantly on increasing the portion of PANI in the composite up to 80%, suggesting that C-TRG and the enclosed PANI particles lead to synergistic capacitive behavior during the charge–discharge cycles. The C_{sp} based on the galvanostatic charge–discharge curve was obtained using the following eqn (3):

$$C_{sp} = (I \times \Delta t)/(\Delta E \times m) \quad (3)$$

where I is the discharge current (A), Δt is the discharge time (s), ΔE is the voltage difference (V), and m is the total active mass of the electrode (g). The C_{sp}s were calculated using eqn (3): 60.58 (TRG), 84.85 (C-TRG), 155.82 (PANI), 118.44 (G80/P20), 237.58 (G40/P60), and 290.17 F g^{-1} (G20/P80) (Fig. 9c). The C_{sp} values and its change pattern were similar to those measured using the CV test.

Finally, the cyclic stability was assessed over 500 cycles at a constant discharging current density of 3 A g^{-1} (Fig. 9d). TRG

and C-TRG exhibited stable performance with ~5% capacitance loss after 500 cycles, whereas capacitance retention of the pure PANI particles decreased significantly to 59.8%. Interestingly, the capacitance retention of the C-TRG/PANI composite electrodes after 500 cycles increased steadily from that of PANI (59.8%) to 87.6% (G80/P20) with increasing C-TRG content in the composite. This result demonstrates that the continuous graphene networks can compensate for the instability of PANI particles, resulting in enhanced long-term stability with excellent electrochemical performance for the supercapacitor.

Recent reports about the electrode based on the graphene/PANI composite are summarized in the ESI (Table S1†). Even though our hybrid electrodes do not possess the highest value of specific capacitance, our amino acid-modified graphene is homogeneously interconnected with PANI particles, resulting in effective preservation of electrochemical performance of the PANI electrode. Thus, continuous networks of the PANI/graphene composite exhibited low internal resistance and highly improved cycle stability during the charge/discharge process.

Conclusion

FTIR, elemental analysis, and XPS showed that simple heating of a well-mixed graphene/potassium 6-aminocaproate mixture in the solid state could effectively induce a reaction between potassium 6-aminocaproate and the epoxide group on graphene, which had been prepared by the thermal reduction of GO. The Raman spectra showed that the modification reaction did not damage the conjugated sp^2 C=C bond network of graphene. The carboxylate groups attached to graphene by a simple modification reaction with potassium 6-aminocaproate made graphene easily dispersible in water, which was stable for more than two months. The negatively charged water-dispersible graphene was efficiently mixed with positively charged, micron-size PANI particles by simple physical mixing of both aqueous dispersions. The energy storage capacities of the composites for supercapacitor applications were mostly higher than those of modified graphene or PANI themselves. This synergistic effect on energy storage was most evident at a graphene/PANI composition of 20/80 by weight. At graphene contents lower than this, the network of the graphene enclosing PANI particles developed imperfectly, and at higher contents, almost all PANI particles were completely encapsulated with graphene sheets. These results suggest that the network structure of modified graphene embedded with PANI particles, and the PANI particles which are not encapsulated completely with graphene but are contactable with the electrolyte are requisites for promoting the synergistic effect. In addition, the graphene network effectively compensated for the instability of PANI particles at repeated charge–discharge cycles.

Acknowledgements

This research study was supported by the Basic Science Research Program through the National Research Foundation of Korea (NRF) funded by the Ministry of Education (NRF-2013R1A1A2004823). T. Lee and B. S. Kim were supported by the National Research Foundation of Korea (NRF) grant (2012R1A1A2040782), by the Development Program of the Korea Institute of Energy Research (KIER) (B4-2424) and by the BK21 Plus funded by the Ministry of Education, Korea (10Z20130011057).

Notes and references

1 C. N. R. Rao, K. Biswas, K. S. Subrahmanyam and A. Grovindaraj, *J. Mater. Chem.*, 2009, **19**, 2457–2469.
2 M. J. McAllister, J.-L. Li, D. H. Adamson, H. C. Schniepp, A. A. Abdala, J. Liu, M. Herrera-Alonso, D. L. Milius, R. Car and R. K. Prud'homme, *Chem. Mater.*, 2007, **19**, 4396–4404.
3 H. Kim and C. W. Macosko, *Macromolecules*, 2008, **41**, 3317–3327.
4 P. Steurer, R. Wissert, R. Thomann and R. Mülhaupt, *Macromol. Rapid Commun.*, 2009, **30**, 316–327.
5 T. Ramanathan, A. Abdala, S. Stankovich, D. Dikin, M. Herrera-Alonso, R. Piner, D. Adamson, H. Schniepp, X. Chen and R. Ruoff, *Nat. Nanotechnol.*, 2008, **3**, 327–331.
6 H. C. Schniepp, J.-L. Li, M. J. McAllister, H. Sai, M. Herrera-Alonso, D. H. Adamson, R. K. Prud'homme, R. Car, D. A. Saville and I. A. Aksay, *J. Phys. Chem. B*, 2006, **110**, 8535–8539.
7 D. A. Nguyen, Y. R. Lee, A. V. Raghu, H. M. Jeong, C. M. Shin and B. K. Kim, *Polym. Int.*, 2009, **58**, 412–417.
8 S. Park, J. An, I. Jung, R. D. Piner, S. J. An, X. Li, A. Velamakanni and R. S. Ruoff, *Nano Lett.*, 2009, **9**, 1593–1597.
9 H. B. Lee, A. V. Raghu, K. S. Yoon and H. M. Jeong, *J. Macromol. Sci., Part B: Phys.*, 2010, **49**, 802–809.
10 Y. Si and E. T. Samulski, *Nano Lett.*, 2008, **8**, 1679–1682.
11 C. Shan, H. Yang, D. Han, Q. Zhang, A. Ivaska and L. Niu, *Langmuir*, 2009, **25**, 12030–12033.
12 H. Yang, C. Shan, F. Li, D. Han, Q. Zhang and L. Niu, *Chem. Commun.*, 2009, **26**, 3880–3882.
13 S. Stankovich, R. D. Piner, X. Chen, N. Wu, S. T. Nguyen and R. S. Ruoff, *J. Mater. Chem.*, 2006, **16**, 155–158.
14 Y. Xu, H. Bai, G. Lu, C. Li and G. Shi, *J. Am. Chem. Soc.*, 2008, **130**, 5856–5857.
15 J. Geng and H.-T. Jung, *J. Phys. Chem. C*, 2010, **114**, 8227–8234.
16 S. Villar-Rodil, J. I. Paredes, A. Martínez-Alonso and J. M. Tascón, *J. Mater. Chem.*, 2009, **19**, 3591–3593.
17 M.-C. Hsiao, S.-H. Liao, M.-Y. Yen, P.-I. Liu, N.-W. Pu, C.-A. Wang and C.-C. M. Ma, *ACS Appl. Mater. Interfaces*, 2010, **2**, 3092–3099.
18 T. D. Dao, H.-I. Lee, H. M. Jeong and B. K. Kim, *Colloid Polym. Sci.*, 2013, **291**, 2365–2374.
19 V. H. Pham, T. T. Dang, S. H. Hur, E. J. Kim and J. S. Chung, *ACS Appl. Mater. Interfaces*, 2012, **4**, 2630–2636.
20 J. Yang, X. Yan, M. Wu, F. Chen, Z. Fei and M. Zhong, *J. Nanopart. Res.*, 2012, **14**, 717.
21 H. Zhang, Q. Zhao, S. Zhou, N. Liu, X. Wang, J. Li and F. Wang, *J. Power Sources*, 2011, **196**, 10484–10489.

22 L. Lai, H. Yang, L. Wang, B. K. Teh, J. Zhong, H. Chou, L. Chen, W. Chen, Z. Shen and R. S. Ruoff, *ACS Nano*, 2012, **6**, 5941–5951.
23 L. Mao, K. Zhang, H. S. O. Chan and J. Wu, *J. Mater. Chem.*, 2012, **22**, 80–85.
24 B. Ma, X. Zhou, H. Bao, X. Li and G. Wang, *J. Power Sources*, 2012, **215**, 36–42.
25 N. A. Kumar, H.-J. Choi, Y. R. Shin, D. W. Chang, L. Dai and J.-B. Baek, *ACS Nano*, 2012, **6**, 1715–1723.
26 J. Zhang and X. Zhao, *J. Phys. Chem. C*, 2012, **116**, 5420–5426.
27 J. An, J. Liu, Y. Zhou, H. Zhao, Y. Ma, M. Li, M. Yu and S. Li, *J. Phys. Chem. C*, 2012, **116**, 19699–19708.
28 Q. Wu, Y. Xu, Z. Yao, A. Liu and G. Shi, *ACS Nano*, 2010, **4**, 1963–1970.
29 J. T. Choi, D. H. Kim, K. S. Ryu, H.-I. Lee, H. M. Jeong, C. M. Shin, J. H. Kim and B. K. Kim, *Macromol. Res.*, 2011, **19**, 809–814.
30 T. Lee, T. Yun, B. Park, B. Sharma, H.-K. Song and B.-S. Kim, *J. Mater. Chem.*, 2012, **22**, 21092–21099.
31 D. Boukhvalov and M. Katsnelson, *Nano Lett.*, 2008, **8**, 4373–4379.
32 D. Konatham and A. Striolo, *Nano Lett.*, 2008, **8**, 4630–4641.
33 B. C. Smith, *Infrared spectral interpretation: a systematic approach*, CRC press, 1999.
34 V. H. Pham, S. H. Hur, E. J. Kim, B. S. Kim and J. S. Chung, *Chem. Commun.*, 2013, **49**, 6665–6667.
35 M. H. Ahmed, J. A. Byrne, J. McLaughlin, A. Elhissi and W. Ahmed, *Appl. Surf. Sci.*, 2013, **273**, 507–514.
36 B. Krauss, T. Lohmann, D.-H. Chae, M. Haluska, K. von Klitzing and J. H. Smet, *Phys. Rev. B: Condens. Matter Mater. Phys.*, 2009, **79**, 165428.
37 C.-Y. Su, Y. Xu, W. Zhang, J. Zhao, X. Tang, C.-H. Tsai and L.-J. Li, *Chem. Mater.*, 2009, **21**, 5674–5680.
38 D.-W. Wang, F. Li, J. Zhao, W. Ren, Z.-G. Chen, J. Tan, Z.-S. Wu, I. Gentle, G. Q. Lu and H.-M. Cheng, *ACS Nano*, 2009, **3**, 1745–1752.
39 C.-C. Hu and J.-Y. Lin, *Electrochim. Acta*, 2002, **47**, 4055–4067.
40 Y. Wang, Z. Shi, Y. Huang, Y. Ma, C. Wang, M. Chen and Y. Chen, *J. Phys. Chem. C*, 2009, **113**, 13103–13107.
41 C. Liu, Z. Yu, D. Neff, A. Zhamu and B. Z. Jang, *Nano Lett.*, 2010, **10**, 4863–4868.
42 M. D. Stoller and R. S. Ruoff, *Energy Environ. Sci.*, 2010, **3**, 1294–1301.

